Enzyme Activity Regulates Substrate Diffusion by Modulating Viscosity in Crowded Milieu

Alessandro Bevilacqua[1], Mauricio Rios Maciel[2], Stefano Pascarelli[1], Mirco Dindo[1], Amy Q. Shen[2,*], and Paola Laurino[1,3,*]

[1]Protein Engineering and Evolution Unit, Okinawa Institute of Science and Technology Graduate University, Onna, 904-0412, Okinawa, Japan.

[2]Micro/Bio/Nanofluidics Unit, Okinawa Institute of Science and Technology Graduate University, Onna, 904-0412, Okinawa, Japan.

[3]Institute for Protein Research, Osaka University, Suita, 565-0871, Japan

*Corresponding author. Email: paola.laurino@oist.jp, amy.shen@oist.jp.

Abstract

Enzymatic activity and its tight regulation are fundamental for cellular metabolism and life. While classical models of enzyme kinetics explain the behaviour of enzymes in buffer solutions, there are elusive properties that emerge from enzymes in their native, crowded environment. In this study, we harness liquid-liquid phase separation (LLPS) to create *in vitro* droplets that mimic cytosolic protein crowding, offering a unique window to understand enzyme kinetics within well controlled microenvironments. We discover that the enzyme self-regulates its activity by modifying the shear viscosity of both the protein-rich droplets and the surrounding bulk solution. Through microscopy and rheology techniques, we discovered a significant correlation between enzyme activity and the shear viscosity of the droplets and bulk solution, influencing substrate diffusion. Our findings suggest that enzymes control their activity, influencing the organization and dynamics of macromolecular crowding within droplets. These results provide new insights into how enzymes regulate both their physical environment and metabolic processes in cell.

Introduction

The physical properties of the cytosol play a crucial role in organizing various cellular processes, including microtubule formation (1), mitosis (2), metabolite diffusion rates (3 , 4), and sensing (5, 6). Additionally, cells dynamically adjust cytosolic properties in response to environmental and cellular cues, such as temperature changes, osmotic stress, starvation, low ATP levels, and metabolic activity. These adaptations are often referred to as liquid to glass-like transition (7–9), viscosity changes (10–12), and viscoadaptation (13, 14). Despite the importance of cytosolic physical properties, measuring how cellular catalytic processes affect cellular viscosity in vivo poses a paramount challenge due to the complexity and interconnectivity of the cellular environment.

Enzymes play an essential role in various life processes, and their activity must be precisely regulated to ensure proper cellular function (15–23). Traditional regulation mechanisms focus on modulating enzyme abundance and catalytic efficiency (24–26). Recent enzyme kinetics studies have highlighted the importance of enzyme assemblies and liquid-liquid phase separation (LLPS) in orchestrating enzyme activity and metabolic fluxes (27–34). In vitro, the physical properties of a solution, such as viscosity and molecular crowding, are known to influence enzyme activity by altering substrate diffusion rates and enzyme dynamics (35–40). However, how enzyme activity itself influences the viscosity of its surrounding medium remains an open question. It is important to recognize that in vitro buffer conditions differ significantly from the complex environment of the cytosol (41). Therefore, developing an in vitro system that accurately replicates the cellular environment is crucial for understanding the role of enzyme activity in modulating cytosolic viscosity.

Liquid-liquid phase separation (LLPS) in vitro systems offer a valuable tool for mimicking cytosolic complexity. They have been utilized to study various cellular phenomena, including enzyme kinetics (33, 42–44), coacervate formation and nucleation (45–48), cell growth (49), protein-membrane interactions (50, 51), molecular diffusion (52), enzyme-driven motion and migration (53, 54). Despite the availability of LLPS systems containing enzymes, studying the perturbation of their physical properties presents challenges due to LLPS poor stability (55–57). Nevertheless, LLPS in vitro systems remain a key approach for exploring the intricate relationship between cellular viscosity and enzyme activity.

Here, we discovered that enzyme activity drives the viscosity of its environment, influencing substrate diffusion and enzyme kinetics. We used a Polyethylene glycol - Bovine Serum Albumin (PEG-BSA) system (43) to generate protein droplets by LLPS, that mimics cytosolic protein crowding concentration (Fig. 1 A). The enzyme β-galactosidase was chosen for this study because of its ability to act on a wide range of reaction substrates. Within our droplets, β-galactosidase activity was modulated by using different substrates (exhibiting different turnover numbers) or enzyme concentrations. Through FRAP and microrheology experiments, we demonstrated that changes in enzyme activity proportionally alter the viscosity of the droplet phase. Additionally, rheological analysis revealed that the enzyme also modulates the viscosity of the surrounding solution. Furthermore, we observed that decreased droplet shear viscosity enhances substrate diffusion by up to three-fold (Fig. 1 B). This study presents the first direct measurement of medium shear viscosity regulated by enzyme activity, highlighting how enzymes can self-regulate their function by adjusting the physical properties of the crowded environment (Fig. 1).

Results

Enzyme kinetic characterization in the droplets system.

To investigate how enzyme activity is influenced by a protein- crowded environment, we utilized a PEG-BSA droplet system (43) to assess the activity of β-galactosidase with various substrates (see reaction scheme in Fig. S1). The buffer conditions of the PEG-BSA system were optimized (see Materials and Methods) to enhance the partitioning of β-galactosidase into the droplets (Fig. S2). The system was characterized to determine the phase composition and droplet volume fraction under different buffer conditions. Inside the droplets, the BSA concentration is 6.6±0.5 mM, the PEG concentration is 2.8±0.3 % (w/w), and the droplets comprise 3.3±0.5 % of the total mixture volume (Fig. S3).

Consequently, the enzyme concentration within the droplets is 30 times higher than the overall solution concentration. The enzyme activity was evaluated for the enzyme placed both within the droplets and in the PEG phase only (see Materials and Methods). We examined the Michaelis-Menten kinetics of β-galactosidase with three different substrates: DDAO-gal, D-lactose, and ONP-gal. The kinetic parameters for β-galactosidase on these three substrates were derived from Michaelis-Menten kinetics (Figs. S4-S6) and are summarized in Table 1.

For all three substrates tested, there are negligible changes in the Km values for the enzyme localized either in the droplets (1.5±0.4, 10.8±3.8 and 1.3±0.3 mM for DDAO-gal, D-lactose and ONP-gal, respectively) or the PEG phase (1.3±0.6, 11.3±2.2 and 1.5±0.2 mM for DDAO-gal, D-lactose and ONP-gal, respectively). With different reaction substrates, the enzyme shows different turnover number (kcat) in both the droplet and PEG phase. Specifically, inside the droplets, the enzyme show a kcat value of 210±28, 72±9 and 502±33 sec^{-1} for DDAO-gal, D-lactose and ONP-gal respectively. Similarly, inside the PEG phase the enzyme show a turnover number of 226±42, 85±6 and 763±32 sec^{-1} for DDAO-gal, D-lactose and ONP-gal respectively. Thus, the catalytic efficiency (kcat/Km) of β-galactosidase inside the droplets is 140.1, 6.7, and 386.0 $sec^{-1}{\cdot}mM^{-1}$ for DDAO-gal, D-lactose and ONP-gal respectively. While for β-galactosidase placed in the PEG phase, the catalytic efficiency is 174.1, 7.5 and 508.5 $sec^{-1}{\cdot}mM^{-1}$ for DDAO-gal, D-lactose and ONP-gal respectively (Tab.1).

These results demonstrate that the system has been effectively optimized for analyzing enzyme kinetics across both PEG-rich and droplet phases. Furthermore, by using multiple substrates, we can adjust the catalytic activity (kcat) within the system, which is essential for further analyses. To better understand enzyme activity in crowded environments, it is essential to explore not just the kinetic parameters but also how physical properties like viscosity influence these processes. Enzyme kinetics traditionally focuses on substrate conversion rates and catalytic efficiency. However, in environments where enzyme concentration and substrate interactions are modulated by the medium's viscosity, the reaction dynamics can change significantly. The rheology of the system, particularly the modulation of shear viscosity, becomes a critical factor as it directly affects substrate diffusion and, in turn, the overall rate of enzyme activity. By examining how enzyme activity correlates with viscosity changes, we can gain deeper insight into how enzymes regulate their local environment to optimize catalytic function. This provides a more comprehensive view of how enzymes operate in complex, crowded environments such as those found in living cells.

Enzyme activity tunes the bulk shear viscosity.

We hypothesize that enzyme activity may influence the shear viscosity of the bulk solution, which consists of the entire aqueous solution, including PEG, BSA droplets with concentrated enzyme and reaction substrates (if introduced), see Fig. 1. We approached this by modifying enzyme activity in two ways: altering the enzymatic reaction substrates (ONPG-gal, DDAO-gal, and lactose) and varying the enzyme concentration in the droplets. We employed steady-state shear rheology to measure changes in the shear viscosity of both the bulk solution (including both the droplets and the PEG-rich phase) (Fig. 2 A, B) and the PEG-phase alone (Fig. 2 A, C), in response to enzyme activity.

Steady flow shear rheological measurements were conducted using a strain-controlled rheometer (ARES G2, TA Instruments, USA). The shear viscosity was determined by performing a flow curve at T = 24°C over a shear rate range of $0.1 < \gamma\square < 100\ s^{-1}$. A parallel plate-plate geometry with a diameter of 50 mm and a gap size of 0.3 mm was used, considering the mean droplet diameter of approximately 20 μm. This setup minimized confinement effects and ensured a uniform distribution of shear throughout the sample. The bulk solution was diluted 1:10 using PEG phase before performing the experiment. Given the viscosity's dependence on shear rate $\gamma\square$ and the presence of shear thinning (Fig. 2 A), we applied the Carreau-Yasuda model, which provided a reasonable fit to the data, particularly at lower shear rates ($\gamma\square < 10\ s^{-1}$). At higher shear rates ($\gamma\square > 10\ s^{-1}$), the model's predictions diverged, likely due to droplet coalescence, which is not considered in the model. Nonetheless, the model's accuracy at lower shear rates suggests that the zero-shear viscosity (η_0) matches well with our measured value at $\gamma\square = 0.1\ s^{-1}$ ($\eta_0 \approx \eta_{0.1}$).

Then, we adjusted the total enzyme activity in the bulk solution by using different reaction substrates. The shear viscosity was measured with and without enzyme β-galactosidase. We assessed the impact of reaction substrates and products on the bulk solution, as depicted in Fig. 2B. Initially, BSA droplets containing 10 nM β-galactosidase in the bulk solution (300 nM within the droplets) were prepared as previously described. These droplets were subsequently diluted 1:10 in a PEG phase that either contained saturating concentrations of substrates (25 mM ONP-gal, 20 mM D-lactose, and 1 mM DDAO-gal) or solely products (25 mM ONP, 20 mM D-glucose, and 1 mM DDAO).

Figure 2B shows how the zero shear viscosity (η_0) is influenced by enzyme activity (using 1 nM enzyme, final concentration in the bulk solution), compared to conditions with only the reaction substrate or product without the enzyme. The presence of enzyme activity notably reduces (η_0) across various conditions. Specifically, in the bulk solution containing both PEG phase and droplets, η_0 decreases from 0.338 (± 0.054) to 0.024 (± 0.011) Pa·s for ONP-gal, from 0.258 (± 0.057) to 0.179 (± 0.020) Pa·s for lactose, and from 0.250 (± 0.037) to 0.054 (± 0.005) Pa·s for DDAO-gal. This trend indicates a clear reduction in shear viscosity associated with increased enzyme activity, particularly noticeable when the enzyme is combined with DDAO-gal or ONP-gal compared to lactose. Control experiments containing substrates or products without the enzyme do not show this reduction (Fig. 2B), highlighting the enzyme's role in altering shear viscosity of the system.

Building on these findings, we correlated the zero-shear viscosity (η_0) of the enzymatically-active bulk solution (Fig. 2B) and PEG-phase only with the catalytic efficiency (kcat) displayed by different reaction substrates (Fig. 2C). Notably, higher kcat values correspond to a decrease in the zero-shear viscosity. Moreover, we modulated the total enzyme activity by adjusting enzyme concentrations (Fig. 2D), focusing on the reaction substrate ONP-gal, which exhibited the most significant change in η_0. These results reveal a clear trend: as enzyme concentration increases

from 0 to 10 nM in the bulk solution, the measured shear viscosity of the bulk solution decreases (Fig. 2D). In summary, while substrates and products individually impact the shear viscosity of the bulk solution (Fig. 2B), the addition of enzyme activity significantly modifies these effects. Notably, the shear viscosity of the bulk solution decreases as both catalytic efficiency (kcat) and enzyme concentration increase (Fig. 2C,D). This highlights a clear correlation between enzymatic activity and viscosity changes in the bulk solution.

Enzyme activity tunes droplets shear viscosity.

After evaluating the bulk shear viscosity influenced by enzyme activity, we also examined the viscosity changes within the droplet phase (Fig.3A). We used Fluorescent Recovery After Photobleaching (FRAP) and particle-tracking microrheology to assess the shear viscosity of the droplet phase, driven by the challenges of isolating and measuring droplet phase viscosity via conventional shear rheology. The typical volume required for rheometer measurements (approximately 0.6 mL) could result in enzymatic reactions primarily occurring at the interface, as seen in larger droplets (Fig 4) (54). Consequently, we estimated the droplet shear viscosity using particle-tracking microrheology. We tracked the Brownian motion of over 50 fluorescent particles, each with a diameter of 1.1 μm, recorded using a confocal microscope over 15 minutes (SI movies 1-4). These particles were tracked to determine their diffusion coefficient (*D*) in the presence of 25 mM ONP-gal at various concentrations of β-galactosidase (0, 0.03, 0.3, and 3 μM inside the droplets, corresponding to 0, 0.01, 0.1, and 1 nM enzyme in the bulk solution). From this diffusion coefficient, we calculated the viscosity (η) using the Stokes-Einstein equation (see Materials and Methods). As shown in Figure 3C, the η_0 of the droplet phase decreases as the enzyme concentration increases, aligning with our earlier findings from bulk rheology measurements. This approach provides a detailed insight into the localized enzymatic effects within the confined environment of the droplets, distinguishing it from the broader effects observed in the bulk measurements.

We used a FRAP approach to corroborate the trend of the microrheology measurements. For the following experiments, BSA was selected as a molecular tracker because it is not involved in the enzymatic reaction and it is the main component of the droplets. The BSA was labelled with the fluorescent probe Alexa Fluor 488 and was used to generate droplets for the FRAP analysis (SI methods). To confirm that the changes in shear viscosity in the bulk solution are shown in the droplets phase, the FRAP experiment was set up with the same experimental conditions of the shear rheology experiments. For this purpose, droplets containing the same range of enzyme concentration (0-3 μM inside the droplets) in the presence of 25 mM ONP-gal were subjected to FRAP (Fig. 3D and SI movies 5-8). The FRAP half-recovery time was determined from the FRAP recovery curves (Fig. 3E). The results show a faster recovery time associated with a higher active enzyme concentration inside the droplets. Specifically, in the presence of 25 mM ONP-gal the half-recovery time decreased from 54.1±16.4 to 53.0±13.6, 43.2±4.0 to 38.1±6.2 seconds in the range of 0, 0.03, 0.3 and 3 μM β-galactosidase in the droplets, respectively. Without enzymatic activity, the presence of the enzyme (0-3 μM β-galactosidase inside the droplets), the substrate (0-25 mM ONP-gal) or the product only (0-0.5 mM ONP) does not show a significant FRAP half-recovery time change even at the maximum expected product production over the experimental timescale (Fig. S7).

In summary, the modulation of viscosity within the droplets correlates with a reduction in shear viscosity, as demonstrated by particle-tracking microrheology, and faster recovery times observed in FRAP measurements, both of which are associated with increasing enzyme concentrations (Fig. 3C, D). These findings are consistent with bulk rheology results (Fig. 2D), collectively

emphasizing enzyme activity as a key regulator of shear viscosity within its crowded environment.

Viscosity modulation facilitates substrate diffusion.

Although previous enzyme kinetics data are independent of the droplet size (Fig. S8), in larger droplets (diameter ≥ 40μm), substrate diffusion becomes the rate-limiting step of the reaction. Here, we demonstrate how the enzyme activity can counteract these diffusion limitations by reducing the viscosity, which in turn enhances the speed of substrate diffusion.

The reaction substrate selected for this experiment is DDAO-Gal since it a fluorescent molecule that has two different excitation/emission spectra before and after the cleavage of the β bound between the DDAO and the D-galactose molecule (58) by the enzyme (reaction scheme Fig.S1). Thus, the diffusion of the substrate inside of the droplets and the generation/diffusion of the product were tracked over time by exciting the probes at λ_g = 488 nm and λg = 648 nm, respectively (Fig.4A). A calibration curve (Fig.S10) was established to correlate the fluorescence intensity of the substrate and product with their respective concentrations (see Materials and Methods). Subsequently, we examined the diffusion of both substrate and product in droplets ranging in diameter (∅) from 15 to 426 μm, both with and without the presence of the enzyme.

A qualitative comparison of droplets containing 9μM enzyme of a ∅ of 36, 63 and 135 μm showed that the time needed for the reaction product DDAO to be generated in the centre of the droplet increased according to the diameter of the droplet (Fig.4B). The diffusion of substrate and product was then quantitatively evaluated by tracking the fluorescence changes inside the whole droplets over time by using a MathLab script (Fig.S9). Specifically, the movies were recorded for 1500 seconds from the addition of the substrate/product (0.2 mM) to reach the diffusion plateau for droplets of diameter ≤ 100μm (Fig.S9). The concentration rate (here defined as the slope of the linear diffusion phase of the reaction substrate and product) in droplets without enzyme is reported in Fig.4C-D. As expected, the concentration rate of both the substrate and product decrease by increasing the size of the droplets. It is important to specify that the molecular diffusion of the substrate/product molecules is the same in all the different droplets size; but the concentration rate is affected by the surface/volume ratio resulting in a negative correlation between the droplets size and molecular concentration. In detail, the substrate concentration rate halves from droplets of ∅ < 40μm (1.18 ± 0.19μM/sec) to droplets ∅ = 41-100 μm (0.68 ± 0.11μM/sec). The negative trend is confirmed in droplets of ∅ = 101-200μm (0.15 ± 0.04μM/sec) and ∅ > 200μm (0.034 ± 0.002μM/sec). The product experiment shows a slower concentration rate than the substrate, but it follows the same trend of the substrate (Fig.4D). Specifically, the product concentration rate is 0.86±0.13μM/sec, 0.19±0.02μM/sec, 0.063±0.027 μM/sec, and 0.032±0.006 μM/sec for droplets of diameter < 40μm, 41-100 μm, 101-200 μm and > 200 μm, respectively.

The same experiment was repeated by using droplets containing 9 μM β-galactosidase (defined as active droplets) and by adding 0.2 mM DDAO-gal during the imaging process. According to the previous experiment, the substrate concentration rate and related product generation decrease by increasing droplet size (Fig.4E). Specifically, the substrate concentration rate inside the active droplets quickly decreases from 4.28±0.42 to 0.33±0.05, 0.011±0.006, and 0.003±0.002 μM/sec for droplets of a diameter of < 40, 41-100, 101-200, and > 200 μm, respectively. Thus, the active droplet size ranges of 41-100, 101-200 and > 200 μm show a 2-, 13- and 11-fold decrease of substrate concentration rate compared to the size ranges of enzyme-less droplets (Fig.4C). Oppositely, the active droplets smaller than 40 μm showed a three-fold increase in substrate

diffusion (4.28 μM/sec) compared to the enzyme-less droplets (1.18 μM/sec). These results suggest that the diffusion of the substrate is enhanced in enzymatically active droplets. Despite the enhanced substrate diffusion, the enzyme activity limits the substrate propagation in droplets of Ø > 40 μm by consuming the substrate before it fully diffuses inside the droplets. Indeed, the lower substrate concentration is compensated by the same or higher concentration of the product present in active droplets of Ø > 40μm compared to the enzyme-less ones (Fig.4D, F). Specifically, the product generated inside the active droplets per second is 0.532 ± 0.26 μM/sec (for a diameter <40 μm), 0.486 ± 0.15 μM/sec (for a diameter of 41-100 μm), 0.120 ± 0.03 μM/sec (for a diameter 101-200 μm) and 0.030 ± 0.018 μM/sec (for a diameter > 200 μm).

After 10 minutes from the addition of the reaction substrate, the substrate concentration in the active droplets is always lower in the active droplets compared to the enzyme-less droplets, while all size ranges of the active droplets showed higher product concentrations than inactive droplets (Fig.S11). Together, these results confirmed the hypothesis that the generation/diffusion of substrate/product inside the active (enzyme-containing) droplets is faster than the diffusion of substrate/product inside inactive (enzyme-less) droplets.

Moreover, we focused on the initial diffusion of substrate (0-120 sec) in active and enzyme-less droplets of a diameter < 40 μm (Fig.4G). Within the first 100 seconds from the addition of the substrate DDAO-gal, the average concentration of substrate inside the enzymatically active droplets is always higher compared to the enzyme-less droplets. The average concentration of substrate inside enzymatically active droplets stabilizes and starts decreasing (within 50-80 sec) around half the substrate concentration added (0.2 mM DDAO-gal) due to its conversion to the reaction product by the enzymatic activity. To consider in this analysis the fraction of substrate diffused but converted into the reaction product, we reported the sum of the concentration of substrate and product inside enzyme-BSA droplets. Notably, within the first 60-second time points, the sum of the concentration of substrate and product in enzyme-BSA droplets is two- to three-fold higher than the concentration of substrate in inactive droplets. We concluded that this enhanced diffusion of the substrate is due to the viscosity decrease caused by the enzymatic activity in the presence of DDAO-gal shown in Fig.2.

Discussion

This study reveals that enzymes can actively regulate substrate availability by modulating the shear viscosity within their crowded environments. Our experiments utilizing the PEG-BSA system demonstrate the enzyme's capability to dynamically adjust the physical properties of a cytosolic-like environment, showing a direct correlation between increased enzyme activity and decreased viscosity. This represents the first direct measurement of viscosity being modulated by enzyme activity, observed both in localized droplets and in the bulk environment.

Contrary to traditional approaches that rely on molecular diffusion assessments (e.g., FRAP) to infer metabolic activity from cellular viscosity (4, 59), our findings offer empirical evidence linking enzymatic activity to medium viscosity alterations. Our discovery supports strategies observed in both unicellular organisms and multicellular organisms like tardigrades, where increased cellular viscosity aids in slowing down metabolic processes under stress (13, 60). The intracellular viscosity is also modulated during the occurrence of several diseases (61–63) potentially linked to enzymatic activity tuning. Previous studies have primarily focused on how crowding and viscosity influence enzymatic reactions (13, 60) yet the reverse–how enzymatic activity impacts medium viscosity has remained unexplored in vitro. Although enzymatic degradation of molecular crowders has been noted to reduce viscosity (64–66), the isolated effect

of enzymatic activity on medium viscosity has not been documented due to typically low viscosity conditions in standard enzyme kinetics studies. Our research, set in a mimicry of the enzyme's native, crowded cytosolic environment (41), highlights the potential for significant viscosity modulation.

Cytosolic viscosity strongly affects biomolecular diffusion and, consequently, cellular metabolism. Measuring metabolite diffusion in relation to dynamic viscosity in the cellular environment is complex due to interactions within the intricate cellular matrix. Using the PEG-BSA system to mimic a simplified cytosolic environment, we measured how substrate availability is directly modified by enzyme activity, thereby changing the shear viscosity of the crowded droplet.

Overall, this study uses a comprehensive approach to link a molecular-level phenomenon (enzymatic activity) to its macroscale (viscosity changes) and mesoscale consequences (substrate and product diffusion), ultimately affecting enzymatic activity itself (substrate availability).

This phenomenon may lead to a form of enzyme self-regulation, where the enzyme modulates its own activity by altering the local viscosity, thereby affecting the diffusion and availability of its substrates. This mechanism appears particularly significant in biological-range droplets (< 40 μm), suggesting a size-dependent effect likely influenced by the surface-to-volume ratio, which might impact substrate diffusion before reaching droplet centers.

The manuscript proposes that the enzyme's activity influences the organization and dynamics of the crowding agents (BSA) within the droplets, leading to changes in viscosity. It's possible that the binding of substrates or the release of products alters the enzyme's conformation or interactions with BSA, affecting the overall packing and mobility of molecules within the droplet. Further investigations into specific enzyme-substrate/product-BSA interactions could elucidate the precise molecular mechanisms underlying this behavior.

The interplay between crowding, viscosity, and enzymatic activity holds profound implications for cellular processes. Enzymes emerge not just as catalysts but as regulators capable of controlling the spatiotemporal dynamics of biomolecular condensates, essential for organizing cellular components and managing biochemical reactions within specific locales.

In conclusion, our study uncovers a novel aspect of enzyme behavior: self-regulation through viscosity modulation. Such insights highlight the potential for enzymes to exert localized control over their activity by manipulating the local viscosity, thereby influencing the diffusion and availability of substrates. This discovery opens avenues for further exploration into how metabolic enzymes might orchestrate cellular viscosity to regulate cellular reorganization and enzyme activity.

This work significantly advances our understanding of the molecular mechanisms at play within crowded cellular environments, highlighting the critical role of enzymes in modulating cellular viscosity and offering a new perspective on the interconnectivity of cellular reorganization, enzyme regulation, and viscoadaptation. Our findings pave the way for future studies aimed at unraveling the complexities of enzyme-mediated viscosity changes and their implications for cellular metabolism and physiology.

Materials and Methods

Materials.

Polyethylene glycol (PEG) 4000 Da (A16151) was purchased from Alpha-Aesar. Bovine serum albumin (BSA) (A7638), 3-(Trimethoxysilyl)propylmethacrylate (440159), 2-Hydroxy-4'-(2-

hydroxyyethoxy)-2-methylpropiophenone (410896), Poly(ethylene glycol) diacrylate (PEGDA) 700 Da (455008) and D-glucose (G8270), β-galactosidase (G5635), potassium phosphate dibasic trihydrate (60349), horse-radish peroxidase (P8375), D-lactose (61339) were purchased from Sigma-Aldrich. Alexa Fluor 488 Microscale Protein Labeling Kit (A30006), Fluoro-Max red fluorescent particle (R0100), (9H-(1,3-Dichloro-9,9-Dimethylacridin-2-One-7-yl) -D-Galactopyranoside) (D6488) were purchased from Thermo Fischer Scientific. 9H-(1,3-dichloro-9,9-dimethylacridin-2-one) (DDAO) was purchased from Setareh Biotech. Potassium phosphate monobasic (42420) was purchased from Acros Organics. Deuterium oxide (D2O) (DE50B) was purchased from Apollo. N,N-dimethylformamide (DMF) (D119) was purchased from Fisher Chemicals. O-dianisidine (119-90-4) was purchased from Tokyo Chemical Industry. ONP-gal (25027-71), sodium hydroxide (31511-05), magnesium chloride (20909-55) and tris(hydroxymethyl)aminomethane (TRIS, 35406-75), Dimethyl Sulfoxide (DMSO, 08904-85), o-nitrophenol (ONP, 24919-92), glucose oxidase (16831-14) were purchased from Nacalai Tesque. Potassium chloride (163-03545) was purchased from Fujifilm Wako.

PEG-BSA system optimization and characterization.

The droplet solution was optimized in the following buffer conditions: Tris (hydroxymethyl) aminomethane-hydrochloride (TRIS-HCl) 300mM buffer pH 7.0, in the presence of potassium chloride 50 mM, Magnesium dichloride 2 mM, BSA 447 μM and 18% PEG (w/w). Importantly, PEG solution was added last and gently mixed to obtain the BSA droplets solution. The system was characterized by measuring the droplet volume fraction and the concentration of PEG and BSA in both the droplet and PEG-rich phase. In order to measure the droplet volume fraction, 1 ml of droplet solution was prepared and centrifuged for 60 mins and 16000 rcf. The PEG-rich phase (supernatant) was removed and the remaining droplets (bottom phase) were centrifuged for 20 mins at 16000 rcf. Remove the residual PEG-rich phase from the centrifuged droplets. 50 μl of water were added to the droplets and mixed by pipetting. This process dissolves the dense droplets phase and allows the measurement of the volume by pipetting. The BSA and PEG concentrations in the two-liquid phases were quantified as previously reported (43).

Diffusion experiment of DDAO and DDAO-gal in droplets.

Droplets without enzyme were prepared and centrifuged for 20 seconds at 10000 rcf and then resuspended with a pipette tip to obtain bigger droplets. Resuspended droplets (2 μL) were diluted 1:10 with PEG phase, moved into a sample chamber placed on coated glass (43) and imaged by using Zeiss LSM880 microscope. Later, 180 μL of PEG phase containing 0.22 mM DDAO-galactoside or 0.22 mM DDAO were added to the diluted droplets (0.2 mM final concentration). Then, the diffusion of substrate and product inside the droplets of different size have been recorded for 1400 sec using 488-nm, 648-nm laser and bright field channels (Supporting movies 9). The same experiment was repeated by using droplets containing 9 μM β-galactosidase and by adding PEG phase solution containing 0.22 mM DDAO-Gal (0.2 mM final concentration) during the imaging process. The fluorescence intensity was converted into product/substrate concentration by using a calibration curve (see supplementary material).

MatLab script.

Analysis of droplet fluorescence was conducted using self-made Matlab scripts. The elliptical circumference of unmoving droplets was extrapolated from a user-defined selection of points. Then, the concentration of product and substrate were calculated using the experimentally determined calibration curve. For average concentration data, only pixels inside the circumference were considered. The scripts used in the analysis are freely available upon request.

Steady flow shear rheology measurements.

The steady flow shear rheological measurement of the fluid was carried out by using a strain-controlled rheometer (ARES G2, TA instruments, USA). The shear viscosity was obtained by running a flow curve at T = 24°C with a shear rate range of $0.1 < \dot{\gamma} < 100\ s^{-1}$ by using a parallel plate-plate geometry of 50 mm diameter with a gap size of 0.3 mm, chosen in relation to the droplets' mean distribution diameter of ≈ 20 μm to prevent confinement effects and achieve uniform shear distribution. In the first set of experiments in the presence of different substrates, the shear viscosity was measured with and without β-galactosidase, assessing the entire bulk solution (droplets + PEG phase) in the presence of reaction substrate and products. The droplets were prepared as explained previously containing 10 nM enzyme in the bulk solution (300 nM in the droplets). The droplets were then diluted 1:10 (1 nM final enzyme concentration in the bulk solution) using the PEG-phase containing a saturating concentration of the substrate (25 mM ONP-gal, 1 mM D-lactose and 20 mM DDAO-gal) or product (25 mM ONP, 1 mM D-glucose and 20 mM DDAO). The shear viscosity was measured also in the PEG-phase in the presence and absence of the enzyme (1 nM final concentration) in the same substrates/products conditions. Regarding the second set of experiment with different enzyme concentrations, the final volume fraction of the droplets was kept the same, while changing the total enzyme allocated in bulk solution to 100, 10, 1 and 0 nM enzyme (3, 0.3, 0.03 and 0 μM in the droplets respectively). This process ensures to have the same amount of droplets across all experiments, to avoid biases on shear viscosity changes due to droplet fraction. The samples were then diluted 1:10 using PEG-rich phase containing 25 mM ONP-gal. To ensure that the enzymatic reaction achieved its steady state and avoid any diffusion limitations, the mixture was allowed to stabilize for 10 minutes before conducting each measurement. Before the flow curve measurement, a preshear of $0.01\ s^{-1}$ for 60s was carried out for all of the samples to ensure a similar initial state.

Particle-tracking microrheology.

During the droplet preparation as described before, red fluorescent beads of 1.1 μm diameter (Fluoro-Max R0100,Thermo Fisher, USA) were added to the droplets preparation mix before the addition of PEG at a final dilution of 1:5000. This process ensures the selective localization of the fluorescent beads into the droplet phase. The droplets solution were diluted 1:10 and 20 μL of droplets were placed in a sample chamber (43) to be imaged after the addition of 180 μL of PEG-phase containing the selected amount of reaction substrate. The particles were visualized using a spinning disk confocal microscope (Nikon, Andor CSU) with a 20X objective and the particles were excited using a laser of λ_g = 561 nm. The images were recorded on a region of interest (ROI) of 1024 x 1024 where at least 15 particles were present. Several places of the sample were recorded to ensure at least 50 particles per case. The images were captured at an interval of 3 s, for up to 1000 seconds. All microrheology experiments were performed at 25°C. Particle tracking was done by Fiji's TrackMate to generate the tracks (coordinates over time) and custom-written code in Python was used to process the trajectories and obtain the mean squared displacement (MSD) of the particles as a function of time (t):

$$\mathrm{MSD(t)} = [\mathrm{r(t_0)} - \mathrm{r(t_0 + t_1)}]^2 \tag{1}$$

Where the average is performed over particles and times, *r* is the coordinate in x or y, since we are assuming 2D diffusion. Then we estimate the diffusion coefficient (*D*) from the *MSD(t)* by fitting a linear regression of the slope *D = MSD(t)/t*. We fitted the *MSD(t)* data at higher times where we can assume that the particles are in free diffusion. From D we calculate the value of viscosity η with the Stokes-Einstein equation:

$$\eta = \frac{k_B T}{6\pi D a} \tag{2}$$

Where k_B is the Boltzman constant, T is temperature in Kelvin and a is the radius of the particle. We validated the method by accurately measuring the shear viscosity of water by adding red fluorescent particle at a final dilution of 1:5000 (data not shown).

References

1. AT Molines, et al., Physical properties of the cytoplasm modulate the rates of microtubule polymerization and depolymerization. Dev. Cell 57, 466–479 (2022).
2. J Xie, et al., Contribution of cytoplasm viscoelastic properties to mitotic spindle positioning. Proc. Natl. Acad. Sci. 119, e2115593119 (2022).
3. AI Garcıa-Pérez, et al., Molecular crowding and viscosity as determinants of translational diffusion of metabolites in subcellular organelles. Arch. biochemistry biophysics 362, 329–338 (1999).
4. E Puchkov, Intracellular viscosity: Methods of measurement and role in metabolism. Biochem. (Moscow) Suppl. Ser. A: Membr. Cell Biol. 7, 270–279 (2013).
5. LJ Holt, M Delarue, Macromolecular crowding: Sensing without a sensor. Curr. Opin. Cell Biol. 85, 102269 (2023).
6. M Bonucci, T Shu, LJ Holt, How it feels in a cell. Trends Cell Biol. (2023).
7. T Murakami, et al., Als/ftd mutation-induced phase transition of fus liquid droplets and reversible hydrogels into irreversible hydrogels impairs rnp granule function. Neuron 88, 678–690 (2015).
8. A Molliex, et al., Phase separation by low complexity domains promotes stress granule assembly and drives pathological fibrillization. Cell 163, 123–133 (2015).
9. Y Lin, DS Protter, MK Rosen, R Parker, Formation and maturation of phase-separated liquid droplets by rna-binding proteins. Mol. cell 60, 208–219 (2015).
10. PP Gopal, JJ Nirschl, E Klinman, EL Holzbaur, Amyotrophic lateral sclerosis-linked mutations increase the viscosity of liquid-like tdp-43 rnp granules in neurons. Proc. Natl. Acad. Sci. 114, E2466–E2475 (2017).
11. L Guo, J Shorter, It’s raining liquids: Rna tunes viscoelasticity and dynamics of membraneless organelles. Mol. cell 60, 189–192 (2015).
12. H Ohishi, et al., Transcription-coupled changes in higher-order genomic structure and transcription hub viscosity prolong enhancer-promoter connectivity. bioRxiv pp. 2023–11 (2023).
13. LB Persson, VS Ambati, O Brandman, Cellular control of viscosity counters changes in temperature and energy availability. Cell 183, 1572–1585 (2020).
14. H Garcia-Seisdedos, M Heidenreich, ED Levy, Not going with the flow: how cells adapt internal physics. Cell 183, 1462–1463 (2020).
15. RM Perrin, et al., Xyloglucan fucosyltransferase, an enzyme involved in plant cell wall biosynthesis. Science 284, 1976–1979 (1999).
16. EW TAYLOR, Cell motility. J. Cell Sci. 1986, 89–102 (1986).
17. M de La Vega, et al., The deubiquitinating enzyme usp17 is essential for gtpase subcellular localization and cell motility. Nat. communications 2, 259 (2011).
18. BN Kholodenko, Cell-signalling dynamics in time and space. Nat. reviews Mol. cell biology 7, 165–176 (2006).
19. NA Clipstone, GR Crabtree, Identification of calcineurin as a key signalling enzyme in t-lymphocyte activation. Nature 357, 695–697 (1992).
20. BA Pandian, R Sathishraj, M Djanaguiraman, PV Prasad, M Jugulam, Role of cytochrome p450 enzymes in plant stress response. Antioxidants 9, 454 (2020).
21. JT Van Dongen, et al., Regulation of respiration in plants: a role for alternative metabolic pathways. J. plant physiology 168, 1434–1443 (2011).

22. J Wiskich, Control of the krebs cycle in Metabolism and Respiration. (Elsevier), pp. 243–278 (1980).
23. LA Fothergill-Gilmore, PA Michels, Evolution of glycolysis. Prog. biophysics molecular biology 59, 105–235 (1993).
24. B Desvergne, L Michalik, W Wahli, Transcriptional regulation of metabolism. Physiol. reviews 86, 465–514 (2006).
25. V Chubukov, L Gerosa, K Kochanowski, U Sauer, Coordination of microbial metabolism. Nat. Rev. Microbiol. 12, 327–340 (2014).
26. L Gerosa, U Sauer, Regulation and control of metabolic fluxes in microbes. Curr. opinion biotechnology 22, 566–575 (2011).
27. IB Smokers, BS Visser, AD Slootbeek, WT Huck, E Spruijt, How droplets can accelerate reactions coacervate protocells as catalytic microcompartments. Accounts Chem. Res. pp. 1046–1054 (2024).
28. BG O'Flynn, T Mittag, The role of liquid–liquid phase separation in regulating enzyme activity. Curr. opinion cell biology 69, 70–79 (2021).
29. T Ura, et al., Activation of l-lactate oxidase by the formation of enzyme assemblies through liquid–liquid phase separation. Sci. Reports 13, 1435 (2023).
30. LJ Sweetlove, AR Fernie, The role of dynamic enzyme assemblies and substrate channelling in metabolic regulation. Nat. communications 9, 2136 (2018).
31. M DINDO, A BEVILACQUA, P LAURINO, Enzymes and liquid-liquid phase separation: A new era for the regulation of enzymatic activity. Seibutsu Butsuri 63, 12–15 (2023).
32. V Jayaraman, et al., A counter-enzyme complex regulates glutamate metabolism in bacillus subtilis. Nat. chemical biology 18, 161–170 (2022).
33. W Jasinska, et al., Non-consecutive enzyme interactions within tca cycle supramolecular assembly regulate carbon-nitrogen metabolism. Nat. Commun. 15, 5285 (2024).
34. X Zhao, et al., Substrate-driven chemotactic assembly in an enzyme cascade. Nat. Chem. 10, 311–317 (2018).
35. B Gavish, M Werber, Viscosity-dependent structural fluctuations in enzyme catalysis. Biochemistry 18, 1269–1275 (1979).
36. S Uribe, JG Sampedro, Measuring solution viscosity and its effect on enzyme activity. Biol. procedures online 5, 108–115 (2003).
37. JG Sampedro, S Uribe, Trehalose-enzyme interactions result in structure stabilization and activity inhibition. the role of viscosity. Mol. cellular biochemistry 256, 319–327 (2004).
38. WL Sweet, JS Blanchard, Fumarase: viscosity dependence of the kinetic parameters. Arch. biochemistry biophysics 277, 196–202 (1990).
39. L Burin, M del Pilar Buera, β-galactosidase activity as affected by apparent ph and physical properties of reduced moisture systems. Enzym. Microb. Technol. 30, 367–373 (2002).
40. AC Miklos, M Sarkar, Y Wang, GJ Pielak, Protein crowding tunes protein stability. J. Am. Chem. Soc. 133, 7116–7120 (2011).
41. K van Eunen, BM Bakker, The importance and challenges of in vivo-like enzyme kinetics. Perspectives Sci. 1, 126–130 (2014).
42. R Toor, et al., Enzymatic cascade reaction in simple-coacervates. J. Colloid Interface Sci. 629, 46–54 (2023).
43. A Testa, et al., Sustained enzymatic activity and flow in crowded protein droplets. Nat. communications 12, 6293 (2021).
44. T Komachi, S Kawai, Y Hirayama, A Maruyama, N Shimada, Encapsulation in cooling-induced coacervates augments dna enzyme activity. Polym. Chem. 14, 4743–4747 (2023).

45. WK Spoelstra, EO Van Der Sluis, M Dogterom, L Reese, Nonspherical coacervate shapes in an enzyme-driven active system. Langmuir 36, 1956–1964 (2020).
46. H Karoui, MJ Seck, N Martin, Self-programmed enzyme phase separation and multiphase coacervate droplet organization. Chem. Sci. 12, 2794–2802 (2021).
47. KK Nakashima, AA André, E Spruijt, Enzymatic control over coacervation in Methods in enzymology. (Elsevier) Vol. 646, pp. 353–389 (2021).
48. NA Erkamp, et al., Biomolecular condensates with complex architectures via controlled nucleation. Nat. Chem. Eng. pp. 1–10 (2024).
49. C Xu, N Martin, M Li, S Mann, Living material assembly of bacteriogenic protocells. Nature 609, 1029–1037 (2022).
50. A Mangiarotti, et al., Biomolecular condensates interacting with membranes: Wetting, remodeling, and damage stabilization. Biophys. J. 123, 310a (2024).
51. A Mangiarotti, R Dimova, Biomolecular condensates in contact with membranes. Annu. Rev. Biophys. 53 (2024).
52. L Hubatsch, et al., Quantitative theory for the diffusive dynamics of liquid condensates. Elife 10, e68620 (2021).
53. S Song, et al., Engineering transient dynamics of artificial cells by stochastic distribution of enzymes. Nat. communications 12, 6897 (2021).
54. M Dindo, et al., Chemotactic interactions drive migration of membraneless active droplets. J. Am. Chem. Soc. (2024).
55. N Gao, S Mann, Membranized coacervate microdroplets: from versatile protocell models to cytomimetic materials. Accounts Chem. Res. 56, 297–307 (2023).
56. I Gözen, et al., Protocells: Milestones and recent advances. Small 18, 2106624 (2022).
57. E Spruijt, Open questions on liquid–liquid phase separation. Commun. Chem. 6, 23 (2023).
58. CH Tung, et al., In vivo imaging of β-galactosidase activity using far red fluorescent switch. Cancer research 64, 1579–1583 (2004).
59. CA Day, M Kang, The utility of fluorescence recovery after photobleaching (frap) to study the plasma membrane. Membranes 13, 492 (2023).
60. N Møbjerg, et al., Survival in extreme environments–on the current knowledge of adaptations in tardigrades. Acta physiologica 202, 409–420 (2011).
61. M Dessard, JB Manneville, JF Berret, Cytoplasmic viscosity is a potential biomarker for metastatic breast cancer cells. Nanoscale Adv. 6, 1727–1738 (2024).
62. JN Sleigh, et al., Age-specific and compartment-dependent changes in mitochondrial homeostasis and cytoplasmic viscosity in mouse peripheral neurons. Aging Cell p. e14250 (2023).
63. W Wang, Y Liu, J Niu, W Lin, Discriminating normal and inflammatory models by viscosity changes with a mitochondria-targetable fluorescent probe. Analyst 144, 6247–6253 (2019).
64. N Mathlouthi, L Saulnier, B Quemener, M Larbier, Xylanase, β-glucanase, and other side enzymatic activities have greater effects on the viscosity of several feedstuffs than xylanase and β-glucanase used alone or in combination. J. agricultural food chemistry 50, 5121–5127 (2002).
65. FM Larsen, MN Wilson, PJ Moughan, Dietary fiber viscosity and amino acid digestibility, proteolytic digestive enzyme activity and digestive organ weights in growing rats. The J. nutrition 124, 833–841 (1994).
66. HS Levinson, ET Reese, Enzymatic hydrolysis of soluble cellulose derivatives as measured by changes in viscosity. The J. Gen. Physiol. 33, 601 (1950).

Acknowledgments

The research was supported by the Okinawa Institute of Science and Technology Graduate University (OIST) with subsidy funding to P.L., S.Pi. and A.Q.S. from the Cabinet Office, Government of Japan. P.L. thanks the financial support from Takeda Grant. M.D. thanks the financial support from Japan Society for the Promotion of Science (JSPS) for the Kakenhi Early Career Scientist N. 22K15065. The authors thank the fruitful discussions with Dr. Vincenzo Calabrese, and Ms. Arisa Yokokoji. We are grateful for the help provided by the imaging section at OIST; in particular, we thank Paolo Barzaghi for the support with the confocal microscopes. A.B. and M.R. would like to thank A. Toriyama for his works that inspire us to keep pushing forward. The images of the present work were prepared using Biorender.com.

Funding:
Okinawa Institute of Science and Technology
Cabinet Office, Government of Japan.
Takeda Science Foundation
Japan Society for the Promotion of Science (JSPS), Kakenhi Early Career Scientist N. 22K15065

Author contributions: A.B. and P.L. conceived the project. A.B., M.R.M., A.Q.S. and P.L. designed the experiments. A.B. performed the experiments regarding the system optimization, enzyme kinetics, FRAP, substrate diffusion and analyzed the data with P.L. A.B. performed the particle tracking experiment while M.R.M. and A.Q.S. analyzed the experimental data. M.R.M. performed the shear rheology experiments, the particle-tracking microrheology and analyzed the data with A.Q.S. S.P. wrote the code for the substrate diffusion experiments analysis. M.R.M. wrote the code for the micro-rheology analysis. A.B., M.R.M., A.Q.S. and P.L. wrote the first draft of the manuscript. All authors contributed to finalize the manuscript. This project was supervised by P.L.

Competing interests: Authors declare that they have no competing interests.

Data and materials availability: All data are available in the main text or the supplementary materials.

Figures and Tables

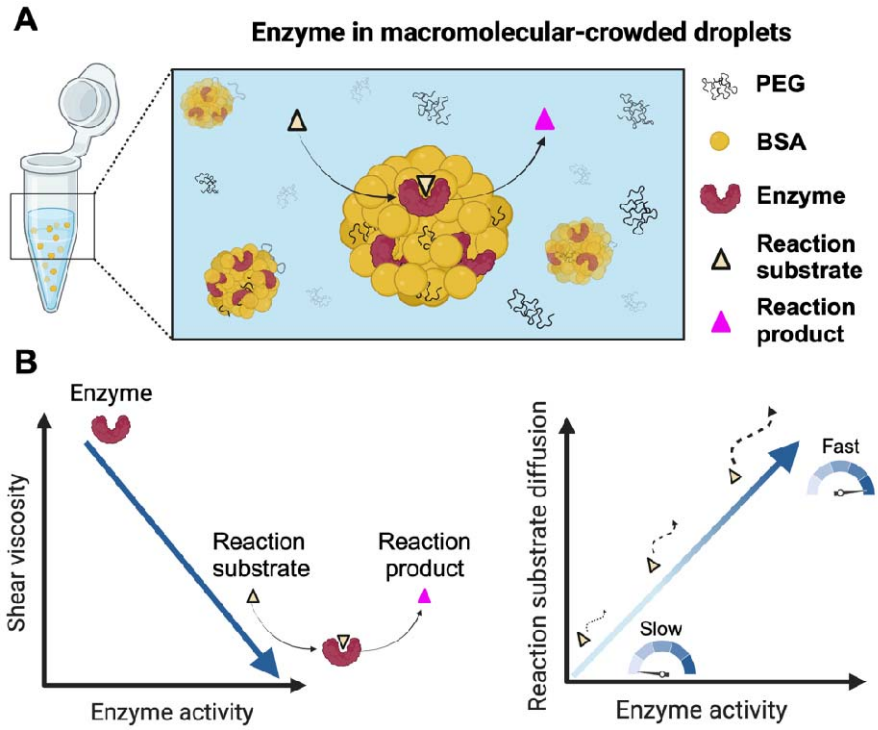

Fig. 1. The enzyme activity modulates the shear viscosity of the droplet crowded environment. (A) Schematic of the PEG-BSA system used to form protein-rich droplets, which replicate cytosolic protein crowding and allow enzyme partitioning. **(B)** Illustration of how enzymatic activity modulates the shear viscosity of both the droplets and the PEG phase, leading to enhanced substrate diffusion. In this context, ”substrate” refers to the specific molecules upon which the enzyme acts, undergoing a chemical reaction to form a product. The efficiency and speed of this reaction are influenced by factors such as enzyme concentration and the viscosity of the surrounding medium.

Substrate	$kcat$ droplet (sec^{-1})	$kcat$ PEG (sec^{-1})	Km droplet (mM^{-1})	Km PEG (mM^{-1})	$kcat/Km$ droplet (sec^{-1} mM^{-1})	$kcat/Km$ PEG (sec^{-1} mM^{-1})
DDAO-gal	210.2±28	226.3±42	1.5±0.4	1.3±0.6	140.1±42	174.1±86
D-lactose	72.0±9.1	85.1±6.1	10.8±3.8	11.3±2.2	6.7±2.5	7.5±1.6
ONP-gal	501.8 ±33	762.8±32	1.3±0.3	1.5±0.2	386.0±93	508.5±71

Table 1. Comparison of the β-galactosidase kinetic parameters obtained in the droplets and in the PEG-rich phase.

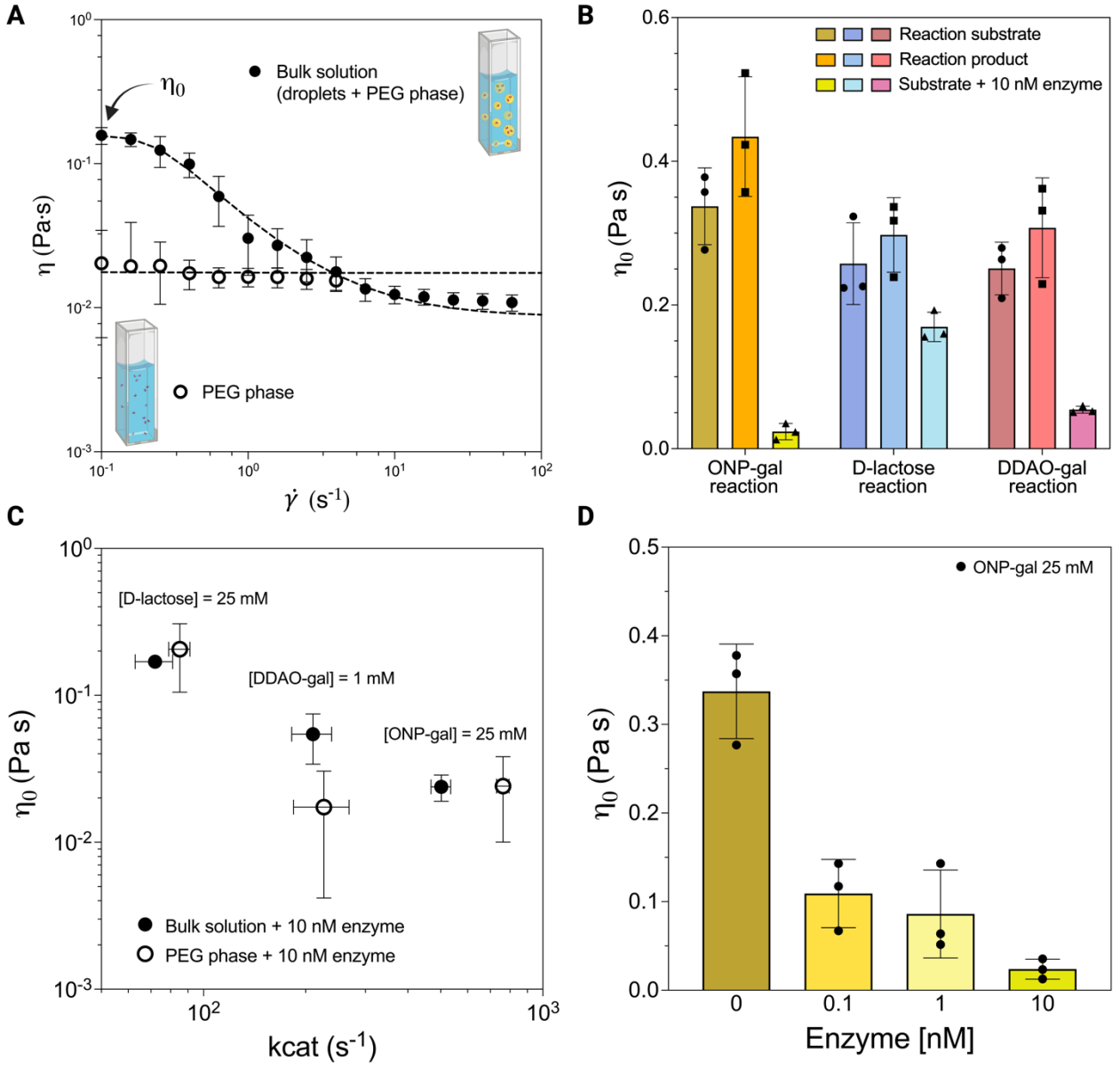

Fig. 2. The enzyme modifies the shear viscosity of the bulk solution. (A) Flow curves of the bulk solution and PEG-phase, showing the viscosity dependance on the shear rate (within a range of = 10^{-1} to 10^{2} s^{-1}. Dotted line represents the Carreau-Yasuda fitting. **(B)** Zero shear viscosity η_0 (at = 0.1 s^{-1}) of the aqueous bulk solution, containing the same amounts of PEG and BSA, was assessed with only reaction substrates at saturating concentrations (25 mM for ONP-gal, 20 mM for D-lactose and 1 mM DDAO-Gal), only products (25 mM ONP, 20 mM D-glucose and 1 mM DDAO) and both reaction substrates plus enzyme (10 nM in the bulk solution). The data represents the mean values ± SD (n=3). **(C)** Logarithmic relationship between η_0 of the bulk solution (black dots) and PEG-phase (grey dots) when the enzyme is active and the corresponding value of catalytic activity (kcat). The data represents the mean values ± SD (n≥3). **(D)** Relationship between the concentration of enzyme in the droplet system and the shear viscosity, tested with 0, 0.1, 1 and 10 nM β-Gal (in the bulk solution) and 25 mM of ONP-gal. The data represents the mean values ± SD (n=3).

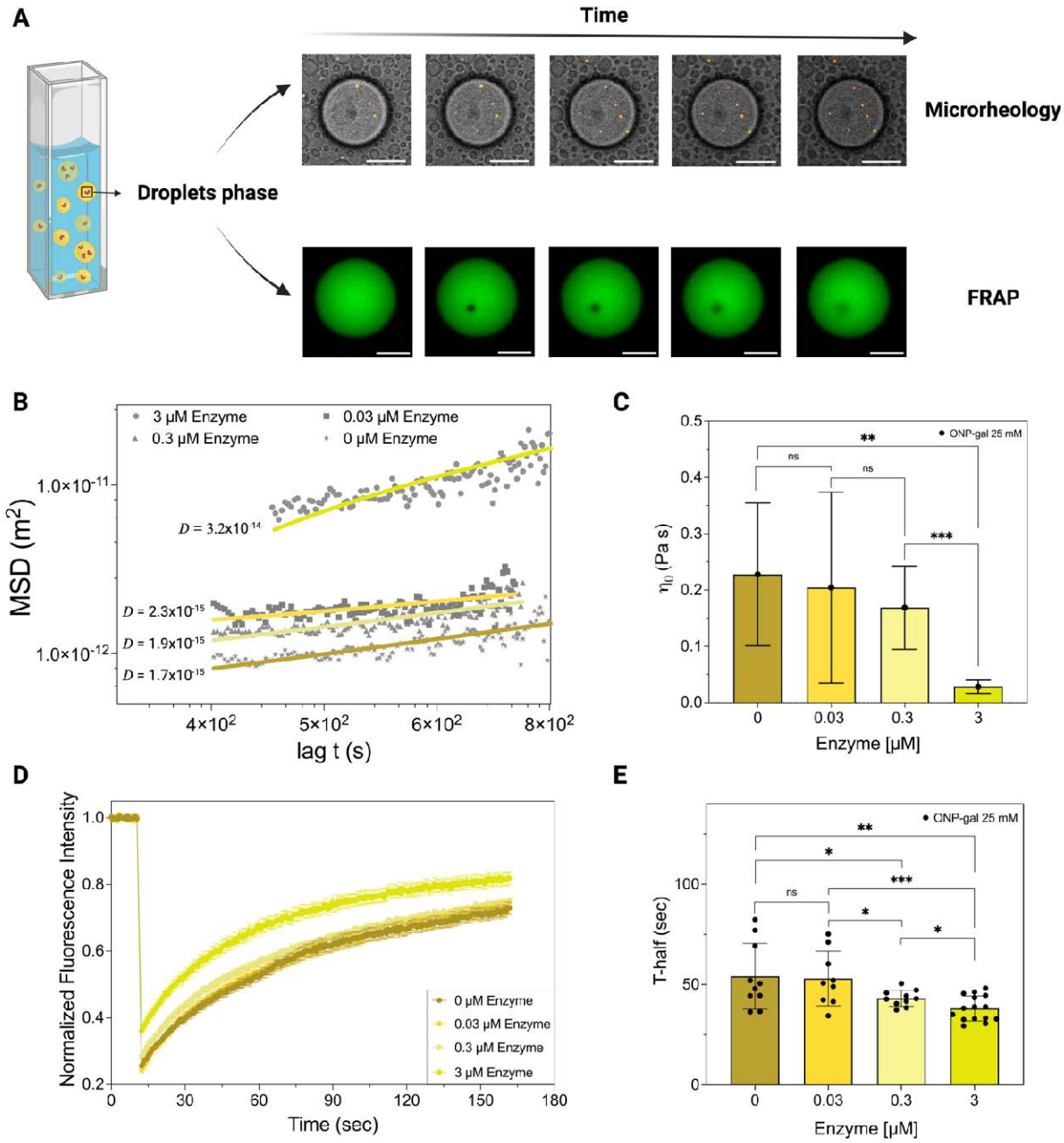

Fig. 3. The enzyme modifies the shear viscosity of the droplets. (A) Experimental setup for viscosity analysis of droplets, utilizing a combination of FRAP and particle-tracking microrheology to measure shear viscosity changes within the droplet phase. Screenshots of the particle-tracking analysis were captured from SI Movie 1 at time points 0, 3.75, 7.5, 11.25, and 15 minutes (scale bar: 50 μm). Representative screenshots from the FRAP experiment were taken from SI Movie 6 at 0, 10, 30, 60, and 120 seconds (scale bar: 10 μm). **(B)** The plot shows the mean squared displacements (MSD) averaged for all the particles at a given lag t for up to 900 s. The linear range assumes a free diffusion regime, where the slope of the linear fit provides an estimate of the diffusion coefficient D (m^2 s^{-1}). Particles were tracked from at least three independent samples ($n \geq 70$ particles). The enzyme concentration ranged from 0 to 3 μM. **(C)** The value of η_0 was derived from particle-tracking microrheology of the droplet phase at varying enzyme concentrations (0–3 μM within the droplets) in the presence of 25 mM ONP-gal. The plot displays the shear viscosity obtained from the fitted diffusion coefficient in panel B, with the standard deviation calculated through error propagation from the slope. Statistical significance was assessed using t-test. P-

values are indicated for comparisons between enzyme concentrations. **$p < 0.01$, ***$p < 0.001$ **(D)** Normalized FRAP data following the photobleaching of (Alexafluor488-labeled) BSA droplets in the presence of 25 mM ONP-gal and a range of β-galactosidase (0-3μM inside the droplets). The fluorescence intensity for each time point of the bleached Region Of Interest (ROI) was normalized by the reference ROI. The data represent the mean ± SEM ($n \geq 9$). **(E)** Relative FRAP half-recovery time of droplets containing a range of 0–100 nM enzyme in the solution (0 − 3 μM β-galactosidase inside the droplets) in the presence of 25 mM ONP-gal. The boxes represent the mean values and the whiskers are the SD ($n \geq 9$). Statistical significance was assessed using t-test. P-values are indicated for comparisons between enzyme concentrations: (0 μM vs 0.03 μM, $p > 0.05$; 0 μM vs 0.3 μM, $p = 0.028$; 0 μM vs 3 μM, $p = 0.001$; 0.03 μM vs 0.3 μM, $p = 0.022$; 0.03 μM vs 3 μM, $p = 0.0007$; 0.3 μM vs 3 μM, $p = 0.016$). *$p < 0.05$, **$p < 0.01$, ***$p < 0.001$.

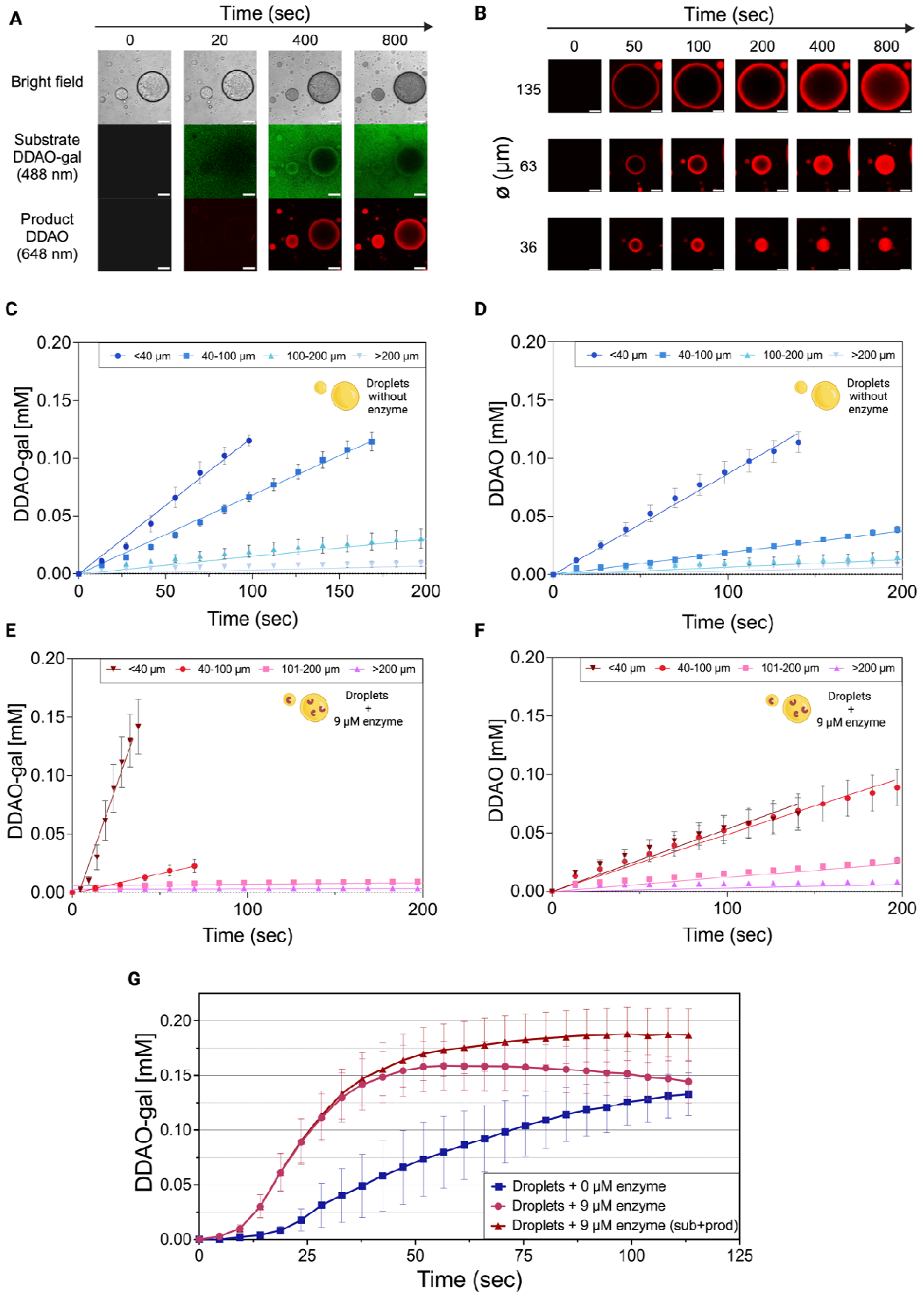

Fig. 4. Substrate diffusion is affected by enzyme-activity-generated shear viscosity changes. (A) Visualization of the reaction occurring inside the droplets at the confocal microscope over time. Top to

bottom: bright field image of the BSA droplets containing 9μM β-galactosidase, the fluorescence of DDAO-galactoside (reaction substrate) excited at λ_g = 488 nm, and the fluorescence of DDAO (reaction product) excited at λ_g = 648 nm. Screenshots from SI movie 9. Scale bar 50 μm. **(B)** Imaging of product generation (excited at 648 nm) inside droplets of different sizes (36, 63, and 135 μm) over 800 sec. Screenshots from SI movie 9. Scale bar 30 μm. **(C)** Diffusion of DDAO-Gal (reaction substrate) inside droplets (without enzyme) of a Ø < 40 (dark blue), 41-100 (blue), 101-200 (light blue) and ≥ 200 μm (light grey). The graph shows the average concentration inside the droplets over 200 seconds from the addition of the reaction substrate. The data points at the diffusion plateau have been removed to fit the diffusion slope of the linear diffusion phase only. The full diffusion curves are reported in Fig.S9. The data represents the mean values ± SEM (n≥4). **(D)** Diffusion of DDAO (reaction product) inside droplets (without enzyme) of a Ø <40 (dark blue), 41-100 (blue), 101-200 (light blue) and ≥ 200 μm (light grey). The graph shows the average concentration inside the droplets over 200 seconds from the addition of the reaction product. The data points at the diffusion plateau have been removed to fit the diffusion slope of the linear diffusion phase only. The full diffusion curves are reported in Fig.S9. The data represents the mean values ± SEM (n≥3). **(E)** Diffusion of DDAO-Gal (reaction substrate) inside droplets (containing 9μM enzyme) of a Ø < 40 (dark red), 41-100 (red), 101-200 (pink) and ≥ 200 μm (light purple). The graph shows the average concentration inside the droplets over 200 seconds from the addition of the reaction substrate. The data points at the diffusion plateau have been removed to fit the diffusion slope of the linear diffusion phase only. The full diffusion curves are reported in Fig.S9. The date represents the mean values ± SEM (n≥5). **(F)** Generation of DDAO (reaction product) inside droplets (containing 9μM enzyme) of a Ø < 40 (dark red), 41-100 (red), 101-200 (pink) and ≥ 200 μm (light purple). The graph shows the average concentration inside the droplets over 200 seconds from the addition of the reaction substrate. The data points at the diffusion plateau have been removed to fit the diffusion slope of the linear diffusion phase only. The full diffusion curves are reported in Fig.S9. The date represents the mean values ± SEM (n≥5). **(G)** Substrate diffusion is improved in enzymatically active droplets. It represents the average substrate concentration inside BSA droplets (blue) and BSA-enzyme droplets (pink) over 115 seconds. In red it is reported the sum of the average concentration of substrate and product inside BSA-enzyme droplets over 115 seconds. The droplets analyzed have a Ø < 40μm. The data represents the mean values ± SEM (n≥6).

Supplementary Materials